6th European Conference on Computational Mechanics (ECCM 6)
7th European Conference on Computational Fluid Dynamics (ECFD 7)
1115 June 2018, Glasgow, UK

DAMAGE DETECTION IN TWO-DIMENSIONAL PLATES VIA INFRARED THERMOGRAPHY

MANUEL PENA[1] **AND MARÍA-LUISA RAPÚN**[1]

[1] E.T.S.I. Aeronáutica y del Espacio, Universidad Politécnica de Madrid
Madrid 28040, Spain
m.penar@alumnos.upm.es, marialuisa.rapun@upm.es

Key words: Infrared Thermography, Non-destructive Testing, Structural Health Monitoring, Inverse Problems, Topological Derivative

Abstract. In this paper, we study the use of active infrared thermography combined with topological derivatives for non-destructive testing of two-dimensional plates. In comparison with other remote testing techniques, like ultrasonics, thermography is less intrusive and non-contact. However, on the other hand, heat transport is a short-range phenomenon and the associated signal-to-noise ratio is less favourable. Despite of this, we will show that the topological derivative is a very powerful tool for processing steady and time-harmonic thermograms to detect inclusions and defects in aluminium plates.

1 INTRODUCTION

Recently, active infrared thermography has been used for the detection and characterization of defects (cavities, cracks, inclusions) in a wide range of fields, including medical [7, 15], building [13], and aircraft structures [8, 19] diagnosis. When applied to damage detection in metallic plates, the method consists on heating the piece to be inspected with some kind of lamp and getting a thermogram (a color image produced by a thermal camera) of the surface of the piece, see Figure 1 for a graphical illustration of the experimental setup. Thermograms are then studied to try to determine the properties of the media that may have gave that response. In this way, information from the whole surface can be collected very fast. In comparison with other remote testing techniques, like ultrasonics, thermographic inspection is safer, more non-intrusive and non-contact [21]. However, on the other hand, heat transport is short range and the associated signal-to-noise ratio is less favourable than in other techniques. Therefore, in many cases, efficient data processing tools are required to successfully interpret thermograms.

In this work, we propose to process steady and time-harmonic thermograms by using a mathematical tool called topological derivative. This derivative can be interpreted as an indicator function of the location, shape and size of the defects. It is a one-step method that does not need any a priori information about the size, number or shape of the defects. It has already been used in a two dimensional thermal propagation problem in an unbounded media in [3] with very good results. For applications to steady problems,

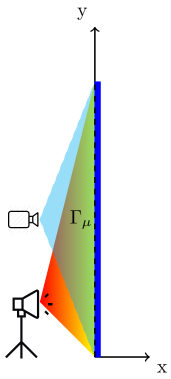

Figure 1: Experimental setup. Both the lamp and the thermal camera are located at the same side of the plate. The thermogram is taken on the side Γ_μ.

like electrical impedance tomography, we refer to [5], and to time-harmonic acoustic and electromagnetic problems we refer to [2, 4, 11] and [14, 17], respectively.

The paper is organized as follows. In Section 2 we formulate the direct and associated inverse thermal problems corresponding to steady and time-harmonic excitations. The topological derivative is defined in Section 3, where we also present the closed-form formulae for the two kind of thermal excitations. Finally, some numerical experiments illustrating the performance of the method are presented in Section 4. Our conclusions are summarized in Section 5.

2 DESCRIPTION OF THE DIRECT AND INVERSE PROBLEMS

We aim at finding the regions of a two-dimensional plate where there can be some interior defects from temperature measurements (thermograms) taken after heating such plate in a controlled and known manner (see Figure 1 for a sketch of the experimental setup). For simplicity, we assume that the plate is rectangular, occupying the region $\Omega = [0, L_x] \times [0, L_y]$, where L_x is assumed to be much smaller than L_y. The temperature $\mathcal{T}(\mathbf{x}, t)$ satisfies the heat equation in Ω,

$$\rho\, c\, \partial_t \mathcal{T} - \nabla \cdot (\kappa \nabla \mathcal{T}) = 0,$$

where, for simplicity, we assume that the mass density ρ, the specific heat capacity c, and the thermal conductivity κ are piecewise constant values, attaining known values inside the defects Ω_i which differ to those in the remaining of the plate $\Omega_e = \Omega \setminus \overline{\Omega}_i$. That is, we assume that

$$\rho\,(\mathbf{x}) = \begin{cases} \rho_{\mathrm{i}}, & \mathbf{x} \in \Omega_{\mathrm{i}} \\ \rho_{\mathrm{e}}, & \mathbf{x} \in \Omega_{\mathrm{e}}, \end{cases} \qquad c\,(\mathbf{x}) = \begin{cases} c_{\mathrm{i}}, & \mathbf{x} \in \Omega_{\mathrm{i}} \\ c_{\mathrm{e}}, & \mathbf{x} \in \Omega_{\mathrm{e}}, \end{cases} \qquad \kappa\,(\mathbf{x}) = \begin{cases} \kappa_{\mathrm{i}}, & \mathbf{x} \in \Omega_{\mathrm{i}} \\ \kappa_{\mathrm{e}}, & \mathbf{x} \in \Omega_{\mathrm{e}}. \end{cases}$$

The plate is supposed to be isolated on its top and bottom boundaries whereas on its left and right sides there is heat transfer to the surrounding air by convection and radiation. Given that the temperatures reached by the plate are not expected to be very far from the ambient temperature T_{air} the radiation process is linearised around it, i.e.

$$\varepsilon\sigma\mathcal{T}^4 \approx \varepsilon\sigma T_{\text{air}}^4 + 4\varepsilon\sigma T_{\text{air}}^3\left(\mathcal{T} - T_{\text{air}}\right),$$

where ε and σ are the surface emissivity and the Stefan-Boltzmann constant, respectively.

In case of steady or time-harmonic excitations, the lamp will be modelled as a point source located at $\mathbf{s} = (s_x, s_y)$ with $s_x < 0$, and mathematically described by a function $q_{\mathbf{s}}$ of the form

$$q_{\mathbf{s}}(x, y) = \frac{P}{2\pi}\frac{x - s_x}{|\mathbf{x} - \mathbf{s}|^2}, \tag{1}$$

where $P > 0$ corresponds to the steady radiant power of the lamp in the steady case, whereas in the time-harmonic case P is the amplitude of oscillation of the radiant power.

In the time-steady case, $\mathcal{T}(\mathbf{x}, t) = T(\mathbf{x})$ and the forward problem reduces to solving

$$\begin{cases} \nabla\cdot(\kappa_{\text{e}}\nabla T) = 0, & \text{in } \Omega_{\text{e}}, \\ \nabla\cdot(\kappa_{\text{i}}\nabla T) = 0, & \text{in } \Omega_{\text{i}}, \\ T^+ - T^- = 0, \qquad \kappa_{\text{e}}\partial_{\mathbf{n}}T^+ - \kappa_{\text{i}}\partial_{\mathbf{n}}T^- = 0, & \text{on } \partial\Omega_{\text{i}}, \\ \partial_y T = 0, & \text{on } y = 0, \quad y = L_y, \\ \kappa_{\text{e}}\partial_x T - AT = -B - \alpha q_{\mathbf{s}}, & \text{on } x = 0, \\ \kappa_{\text{e}}\partial_x T + AT = B, & \text{on } x = L_x, \end{cases} \tag{2}$$

with $A = h + 4\varepsilon\sigma T_{\text{air}}^3$ and $B = hT_{\text{air}} + (\alpha + 3\varepsilon)\sigma T_{\text{air}}^4$, where h is the convective heat transfer coefficient between the plate and the surrounding air and α is the absorptance of that surface.

When the heating is time-harmonic, after a long enough time, the temperature distribution behaves as $\mathcal{T}(\mathbf{x}, t) = \tilde{T}(\mathbf{x}) + \mathfrak{Re}\left(T(\mathbf{x})e^{-i\omega t}\right)$, where $\tilde{T} > 0$ is a steady mean value, $\omega > 0$ is the excitation frequency, and the complex thermal amplitude $T(\mathbf{x})$ solves

$$\begin{cases} \nabla\cdot(\kappa_{\text{e}}\nabla T) + i\omega\rho_{\text{e}}c_{\text{e}}T = 0, & \text{in } \Omega_{\text{e}}, \\ \nabla\cdot(\kappa_{\text{i}}\nabla T) + i\omega\rho_{\text{i}}c_{\text{i}}T = 0, & \text{in } \Omega_{\text{i}}, \\ T^+ - T^- = 0, \qquad \kappa_{\text{e}}\partial_{\mathbf{n}}T^+ - \kappa_{\text{i}}\partial_{\mathbf{n}}T^- = 0, & \text{on } \partial\Omega_{\text{i}}, \\ \partial_y T = 0, & \text{on } y = 0, \quad y = L_y, \\ \kappa_{\text{e}}\partial_x T - AT = -\alpha\, q_{\mathbf{s}} & \text{on } x = 0, \\ \kappa_{\text{e}}\partial_x T + AT = 0, & \text{on } x = L_x. \end{cases} \tag{3}$$

The extra $i\omega\rho c$ term that appears in (3) takes into account the time derivative in the time-harmonic case. On the other hand, the B term is not appearing any more as it is absorbed by the steady value $\tilde{T}(\mathbf{x})$.

After heating the plate (either in a stationary or a time-harmonic way), we will measure the temperature on the side $x = 0$, the same side of Ω that is heated by the lamp. Although actual thermal cameras measure thermal radiation rather than direct temperature, we assume that our thermogram has been already processed to give the measured temperature distribution T^{meas} on $x = 0$ in the stationary case, or the measured complex thermal amplitude T^{meas} on $x = 0$ in the time-harmonic one. Notice that for ease of notation, T^{meas} and T will be either related to problem (2) or (3). Knowing T^{meas}, we aim to find the true defects Ω_i such that the solution T to (2) or (3) agrees with the measured data, namely, such that $T = T^{\text{meas}}$ on $x = 0$. This is a very strict condition taking into account that measurements are expected to contain experimental errors. Furthermore, this inverse problem is non-linear and strongly ill-posed. Therefore, we propose to relax the requirement by searching the set Ω_{i} that minimizes the functional

$$J\left(\Omega \setminus \overline{\Omega}_{\text{i}}\right) = \frac{1}{2} \int_{\{x=0\}} \left|T - T^{\text{meas}}\right|^2 \, \mathrm{d}\ell, \tag{4}$$

where T is the solution to (2) or (3), and T^{meas} is its corresponding processed thermogram. We use the notation $J\left(\Omega \setminus \overline{\Omega}_{\text{i}}\right)$ to highlight that T solves a problem where the defects occupy Ω_i, and also because it is useful to deal with the topological derivative definition, which is given in section 3.

3 TOPOLOGICAL DERIVATIVE

In this section we will explain the general concept of the topological derivative (TD in the sequel) and provide closed-form formulae for it when applied to the functional (4) in both, the steady and the time-harmonic situations.

The TD of a shape functional $\mathcal{J}(\mathcal{R}) = \mathcal{J}(u_{\mathcal{R}})$, where $\mathcal{R}$ is a region in $\mathbb{R}^2$ and $u_{\mathcal{R}}$ is the solution to a PDE problem defined in $\mathcal{R}$, is a scalar field D_T that measures the sensitivity of $\mathcal{J}$ when an infinitesimal ball is located at each point $\mathbf{x} \in \mathcal{R}$ (see [18]). It gives at each point $\mathbf{x} \in \mathcal{R}$ the asymptotic expansion

$$\mathcal{J}\left(\mathcal{R} \setminus \overline{\mathrm{B}}_\epsilon\left(\mathbf{x}\right)\right) = \mathcal{J}\left(\mathcal{R}\right) + D_T\left(\mathbf{x}\right) \mathcal{V}\left(\epsilon\right) + o\left(\mathcal{V}\left(\epsilon\right)\right), \quad \text{as } \ \varepsilon \to 0, \tag{5}$$

where $\mathcal{V}$ is a positive monotonic increasing function such that $\mathcal{V}\left(0\right) = 0$. The function $\mathcal{V}$ is a measure of the size of the ball $\mathrm{B}_\epsilon(\mathbf{x})$, and is chosen such that D_T has non-zero finite values. In our case, we can choose $\mathcal{V}\left(\epsilon\right) = \pi\epsilon^2$. This expansion motivates our reconstruction technique: we will place objects in the regions where the TD will attain pronounced negative values, since in those points the error functional is expected to decrease. Namely, for our considered problems, the true set of defects Ω_i will be approximated as the set

$$\Omega_{\text{app}} := \left\{ \mathbf{x} \in \Omega;\ D_T\left(\mathbf{x}\right) < \lambda \min_{\mathbf{y} \in \Omega} D_T(\mathbf{y}) \right\} \tag{6}$$

where $0 \leq \lambda \leq 1$ is a tunable threshold. In Section 4 we will test the robustness of the method in terms of the choice of λ.

In the next theorems we provide closed-form expressions of the TD of the cost functional (4), which can be derived by using the relationship between shape and topological derivatives, and adjusting the results obtained by one of us in [5] for the steady case, and in [2] for the time-harmonic one.

Theorem 3.1 *For the steady-state case, the TD of the cost function (4) at the point* $\mathbf{x} \in \Omega$ *is given by*

$$D_T(\mathbf{x}) = 2\kappa_{\mathrm{e}}(\kappa_{\mathrm{e}} - \kappa_{\mathrm{i}})(\kappa_{\mathrm{e}} + \kappa_{\mathrm{i}})^{-1}\, \nabla T^0\,(\mathbf{x}) \cdot \nabla V^0\,(\mathbf{x})\,,$$

where T^0 *satisfies*

$$\begin{cases} \nabla \cdot (\kappa_{\mathrm{e}} \nabla T^0) = 0, & \text{in } \Omega, \\ \partial_y T^0 = 0, & \text{on } y = 0, \quad y = L_y, \\ \kappa_{\mathrm{e}} \partial_x T^0 - A T^0 = -B - \alpha q_{\mathbf{s}}, & \text{on } x = 0, \\ \kappa_{\mathrm{e}} \partial_x T^0 + A T^0 = B, & \text{on } x = L_x, \end{cases} \tag{7}$$

and V^0 *solves the following adjoint problem*

$$\begin{cases} \nabla \cdot (\kappa_{\mathrm{e}} \nabla V^0) = 0, & \text{in } \Omega, \\ \partial_y V^0 = 0, & \text{on } y = 0, \quad y = L_y, \\ \kappa_{\mathrm{e}} \partial_x V^0 - A V^0 = T^{\mathrm{meas}} - T^0, & \text{on } x = 0, \\ \kappa_{\mathrm{e}} \partial_x V^0 + A V^0 = 0, & \text{on } x = L_x, \end{cases} \tag{8}$$

Theorem 3.2 *For the time-harmonic case, the TD of the cost function (4) at the point* $\mathbf{x} \in \Omega$ *is given by*

$$D_T\,(\mathbf{x}) = \mathfrak{Re}\left(2\kappa_{\mathrm{e}}(\kappa_{\mathrm{e}} - \kappa_{\mathrm{i}})(\kappa_{\mathrm{e}} + \kappa_{\mathrm{i}})^{-1}\, \nabla T^0\,(\mathbf{x}) \cdot \overline{\nabla V^0\,(\mathbf{x})} + i\omega\,(\rho_{\mathrm{e}} c_{\mathrm{e}} - \rho_{\mathrm{i}} c_{\mathrm{i}})\, T^0\,(\mathbf{x})\, \overline{V^0\,(\mathbf{x})}\right)$$

where T^0 *is the solution to*

$$\begin{cases} \nabla \cdot (\kappa_{\mathrm{e}} \nabla T^0) + i\omega \rho_{\mathrm{e}} c_{\mathrm{e}} T^0 = 0, & \text{in } \Omega, \\ \partial_y T^0 = 0, & \text{on } y = 0, \quad y = L_y, \\ \kappa_{\mathrm{e}} \partial_x T^0 - A T^0 = -\alpha\, q_{\mathbf{s}} & \text{on } x = 0, \\ \kappa_{\mathrm{e}} \partial_x T^0 + A T^0 = 0, & \text{on } x = L_x. \end{cases} \tag{9}$$

and V^0 *solves*

$$\begin{cases} \nabla \cdot (\kappa_{\mathrm{e}} \nabla V^0) - i\omega \rho_{\mathrm{e}} c_{\mathrm{e}} V^0 = 0, & \text{in } \Omega, \\ \partial_y V^0 = 0, & \text{on } y = 0, \quad y = L_y, \\ \kappa_{\mathrm{e}} \partial_x V^0 - A V^0 = T^{\mathrm{meas}} - T^0, & \text{on } x = 0, \\ \kappa_{\mathrm{e}} \partial_x V^0 + A V^0 = 0, & \text{on } x = L_x. \end{cases} \tag{10}$$

Notice that the results in the previous theorems allow us to compute the TD in the whole domain by solving just one forward problem and one adjoint problem which take place in the whole plate Ω, where no defect is present. Therefore, no information about the true number or shape of the searched objects is necessary. Notice also that the measured data T^{meas} enters in the TD in the right hand side at the boundary condition on $x = 0$ in the adjoint problem (8) or (10).

In the case of having multiple experiments either by locating the lamps at different positions or by changing the frequency in the time-harmonic case, we can consider a new cost functional defined as a linear combination of single-lamp functionals and/or single-frequency ones. Then, by linearity, the corresponding TD is nothing but the corresponding linear combination corresponding to individual functionals. If $\left\{D_T^j\right\}_1^{N_{\text{exp}}}$ is a set of N_{exp} independent TDs, then following the ideas in [10], we propose to consider the weighted TD

$$\hat{D}_T(\mathbf{x}) = \sum_{j=1}^{N_{\text{exp}}} \frac{D_T^j(\mathbf{x})}{\left|\min_{\mathbf{y}\in\Omega} D_T^j(\mathbf{y})\right|}, \quad \mathbf{x} \in \Omega, \tag{11}$$

as a new indicator function. Since individual derivatives can attain disparate values, in this way we avoid neglecting the contributions of some lamps and/or frequencies that could be neglected by adding contributions. Furthermore, we expect that the false negatives of one derivative get cancelled with the values of another one.

4 NUMERICAL EXPERIMENTS

In order to test the method, thermograms were generated by solving the corresponding direct problems numerically, using the free FEM solver *FreeFem++* [12] adding to them random noise of 5% in magnitude to both avoid inverse crimes and to test the performance of the method when dealing with noisy data. The direct and adjoint problems involved in the formulae of the TD were also solved by using *FreeFem++*, considering in this case a different mesh of Ω, where no defects were present. All figures in this section were made using the free software package *GNU-octave* [9].

In all experiments, we consider an aluminium plate of dimensions $L_x = 0.01\,\text{m}$ and $L_y = 1\,\text{m}$ with two internal holes consisting of air: a circular hole of radius $2\,\text{mm}$ situated at $(0.005, 0.4)$ and an elliptical one of semi-axes of $2\,\text{mm}$ and $6\,\text{mm}$ situated at $(0.005, 0.7)$. The constants in the model are the following: $\kappa_{\text{e}} = 200\,\text{W/K}$, $\rho_{\text{e}} = 2700\,\text{Kg/m}^2$, $c_{\text{e}} = 900\,\text{J/(Kg}\cdot\text{K)}$, $\kappa_{\text{i}} = 0.025\,\text{W/K}$, $\rho_{\text{i}} = 1\,\text{Kg/m}^2$, $c_{\text{i}} = 1000\,\text{J/(Kg}\cdot\text{K)}$, $\alpha = 0.4$, $\varepsilon = 0.08$, $h = 15\,\text{W/(m}\cdot\text{K)}$, $T_{\text{air}} = 290\,\text{K}$, and $P = 600\,\text{W}$ for the steady-state case and $P = 6000\,\text{W}$ for the time-harmonic one. In both cases, the plates were illuminated at a distance of 15 cm giving temperatures between 300 K in the coldest parts of the plate and 305 K in the hottest ones for the steady-state case and maximum amplitudes of 1 K for the time-harmonic one. In Figure 2a we represent the considered flawed plate and some of the configurations of lamps that will be considered in the forthcoming numerical experiments.

Let us consider first steady-state excitations. In Figure 2b we show the values of the weighted TD indicator function (11) for the ten lamps indicated as black crosses in Figure 2a. We observe that the larger negative values (dark blue colors) concentrate near the defects of the flawed plate, specially in the region occupied by the elliptical defect.

For a better visualization, we show in the upper part of the plots in the subsequent figures the values of $\hat{D}_T$ divided by $|\min_{\mathbf{y}\in\Omega} \hat{D}_T(\mathbf{y})|$ on the side $x = 0$ the y-coordinate. In the bottom of the figures, we represent the (rotated) plate, where the true objects

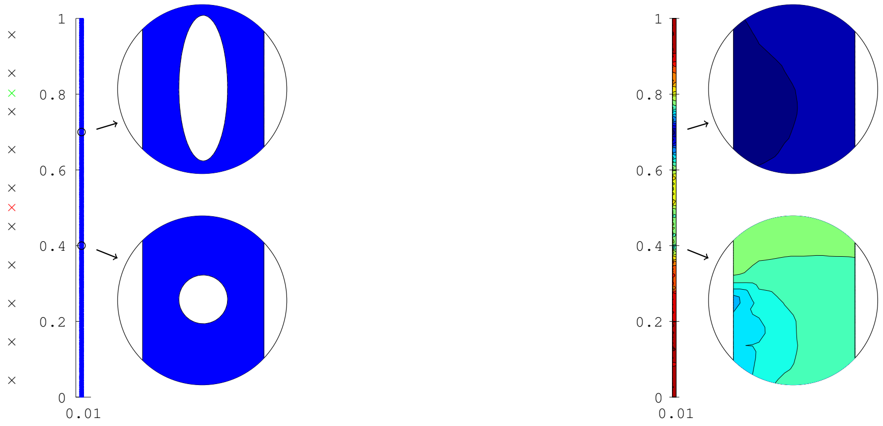

(a) Plate with two defects.

(b) TD field $D_T(x, y)$.

Figure 2: (a) Diagram of the flawed plate and location of some of the lamps considered in the examples ('×' marks). (b) TD field obtained for the steady case when considering the ten lamps located at the points marked in (a) by black crosses.

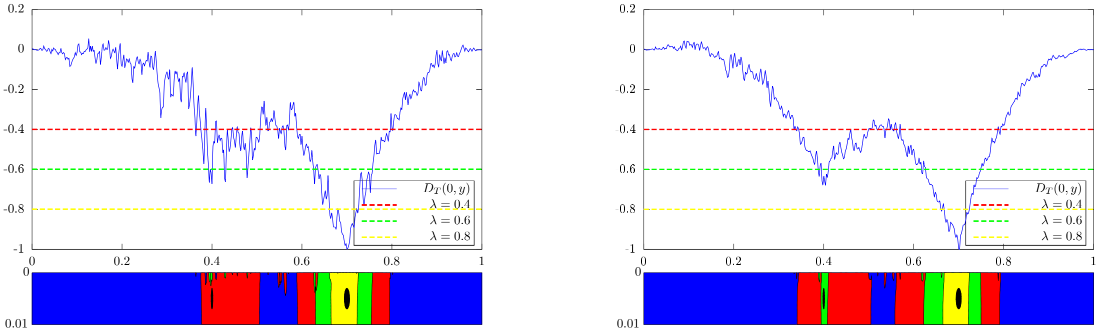

(a) Ten lamps.

(b) Fifty lamps.

Figure 3: Topological derivative and reconstructed objects when considering ten (left plot) and fifty (right plot) steady thermograms.

are represented by black domains, and the reconstructed domains, obtained by selecting different values of λ in (6), are represented by different color regions. The scaling of the plate in the horizontal direction (interval $[0, L_y]$) is different from that in the vertical direction (interval $[0, L_x]$) for a better visualization. Notice that this promotes that the true objects seem to be elliptical. Figure 3a corresponds to the ten lamps indicated as black crosses in Figure 2a. In its bottom part, we observe that the region identified as damaged highly depends on λ. If we choose $\lambda = 0.8$, we obtain the region in yellow. Therefore, we just recover the location of the ellipse, overestimating its size. Decreasing λ to 0.6 (union of yellow and green regions), we highly overestimate the size of the ellipse, and the circular hole is misinterpreted as a collection of tiny objects located close to the side $x = 0$. A further decrease to $\lambda = 0.4$ promotes the reconstruction of two big areas (union of yellow, green and red zones), and furthermore, a new spurious small region between both objects is also identified. Individual contributions are not shown here, but as one can expect, reconstructions are very poor and local minima can be easily misunderstood as spurious objects. Increasing the number of experiments to fifty, reconstructions only improve a bit, as observed in Figure 3b.

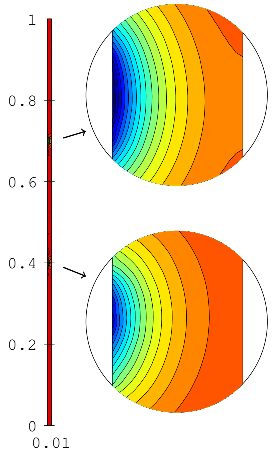

Figure 4: DT field for the harmonic case when considering one lamp and $\omega = 1\,\text{Hz}$.

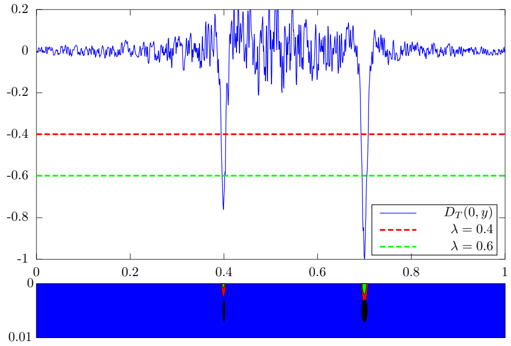

Figure 5: One lamp at $1\,\text{Hz}$

Let us consider now the time-harmonic case. First we inspect the same plate by considering just one lamp, represented by a red cross in Figure 2a, and the frequency $\omega = 1\,\text{Hz}$. In comparison with the steady case, we observe that just one lamp is enough to highly improve the reconstruction, as can be observed in Figures 4 (counterpart of Figure 2b) and 5 (counterpart of Figure 3). We observe that we are able to reconstruct both

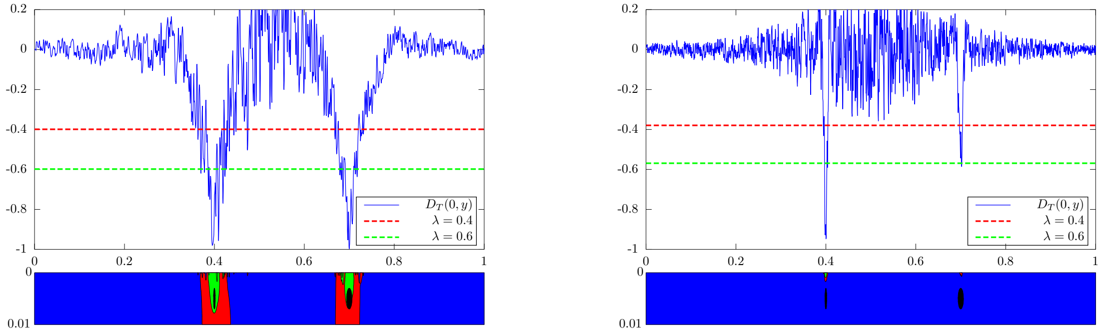

(a) One lamp at 0.1 Hz.

(b) One lamp at 5 Hz

Figure 6: Comparison for two different frequencies.

defects with an accurate estimation of their size for a wide range of values of λ. This means that reconstructions are now very robust with respect to λ, while in the steady case, the size of the reconstructed objects highly depended on it. However, we observe that the TD does not give the correct depth and width of the defects, being always the reconstruction at the surface being inspected. Changing the frequency of study does not amend this problem, as can be seen in Figure 6, which is the counterpart of Figure 5 when replacing $\omega = 1\,\mathrm{Hz}$ by $\omega = 0.1\,\mathrm{Hz}$ and $\omega = 5\,\mathrm{Hz}$. Furthermore, in Figure 6a it can be seen that if we decrease too much the frequency we recover results similar to the ones of the steady-state case, as it could be expected. We also observe that the higher the frequency, the more acute minima. It is also remarkable that depending on the selected frequency, the global minimum of the weighted topological derivative points either at the region where the ellipse is located (which has a larger area) or at the region occupied by the circle (which is closer to the lamp location).

If we combine different frequencies we can cancel out the false local minima much more efficiently than combining positions in the steady state case, as can be seen in Figure 7a where only 10 experiments were needed. We want to empathize that we are considering a favourable situation, because the lamp is located between both objects. If we repeat the same experiment but locating now the lamp at the position indicated as a green cross in Figure 2a, we find the results in Figure 7b. We sharply identify the location and size of the ellipse, but the circular hole is completely missed. Although it is not shown here, if we consider a lamp located at the bottom part of the plate, then the circular hole is well-recovered while the ellipsoidal one is missed. To avoid this problem, and taking into account that we assume no a priori information, we propose to combine DTs corresponding to different positions of the lamp.

In Figure 8a the same 10 frequencies were used but now 5 different positions of the lamp (uniformly distributed all along the height of the plate) were considered. In comparison with Figure 3b, where the same amount of data was used (fifty experiments), it is clear that time-harmonic excitations highly improve reconstructions. However, there is still a

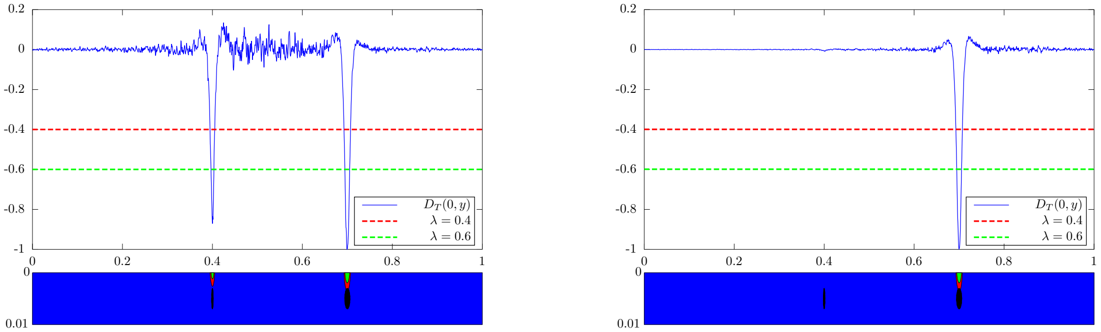

(a) Lamp at the red cross in Figure 2a.

(b) Lamp at the green cross in Figure 2a.

Figure 7: Comparison for two different positions of the lamp. In both cases, ten linear spaced frequencies between 0.8 Hz and 2 Hz were considered.

lack of accuracy in the reconstruction in the x-direction.

Finally, we want to illustrate the performance of the method when dealing with noisy data. In all our previous experiments, thermograms contained a 5% random noise. Increasing this noise to a 20% level, reconstructions are roughly the same, as can be observed in Figure 8b. This means that our method is extremely robust with respect to measurement errors.

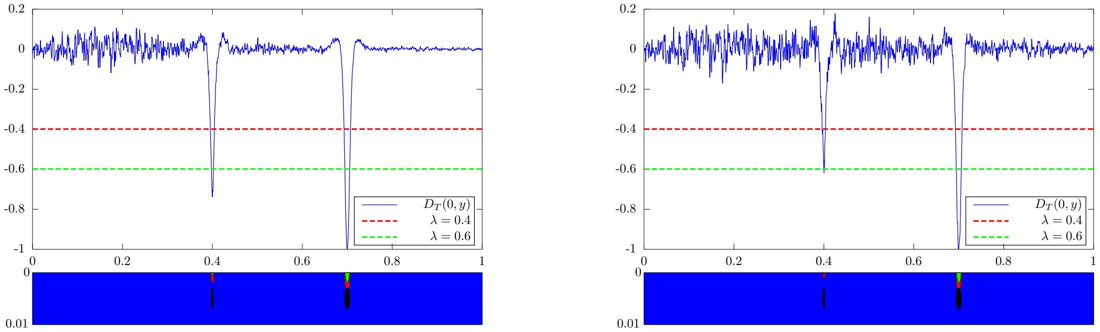

(a) 5% error

(b) 20% error

Figure 8: Comparison for thermograms containing different levels of noise. Thermograms correspond to ten uniformly spaced frequencies between 0.8 Hz and 2 Hz and five lamp position.

5 CONCLUSIONS

Steady and time-harmonic thermograms have been processed by using topological derivatives to detect defects inside a two dimensional plate. The main conclusion is that the proposed methods, specially when dealing with time-harmonic excitations, are able to sharply recover the location in the y-direction and their approximate size. Moreover, the method is extremely robust with respect to noise, which makes it very appealing for future industrial applications. However, the correct position in depth (in the $x-$direction), and the width of the defects is not properly recovered. This fact is inherent to this kind of problems, as already observed in [20]. We believe that this problem can be amended by procesing transient thermograms (obtained by considering general time-dependent thermal excitations). This will be the subject of our future work.

On the other hand, we have used the TD as a one-step indicator function. However, it can be also iteratively used as a gradient-descent method in order to reach the optimal domain, as done in [1, 2, 4]. This strategy could improve reconstructions, increasing, however, the associated computational cost. Our first-stage approximations can also be used as initial guesses for some other iterative methods like level set strategies [16] or shape derivative based algorithms [6].

Acknowledgements. This research has been supported by the Spanish Ministry of Economy and Competitiveness, under Grants TRA2016-75075-R and MTM2017-84446-C2-1-R. We would like to thank M. Higuera, J.M. Perales and J.M. Vega for fruitful discussions.

REFERENCES

[1] Carpio A. and Rapún M.-L. Topological Derivatives for Shape Reconstruction. *Inverse Problems and Imaging. Lecture Notes in Mathematics, 1943.* Springer, Berlin, Heidelberg, 2008.

[2] Carpio A. and Rapún M.-L. Solving inhomogeneous inverse problems by topological derivative methods. *Inverse Problems* (2008) **24**: art. num. 045014.

[3] Carpio A. and Rapún M.-L. Domain reconstruction using photothermal techniques. *Journal of Computational Physics* (2008) **227**:8083–8106.

[4] Carpio A., Johansson B.T. and Rapún M.-L. Determining planar multiple sound-soft obstacles from scattered acoustic fields. *J. Math. Imaging Vision* (2010) **36**:185–199.

[5] Carpio A. and Rapún M.-L. Hybrid topological derivative and gradient-based methods for electrical impedance tomography. *Inverse Problems* (2012) **28**: art. num. 095010.

[6] Cimrak I. Inverse thermal imaging in materials with nonlinear conductivity by material and shape derivative method. *Math. Methods Appl. Sci* (2011) **34**: 2303–2317.

[7] Costello J.T., McInerney C.D., Bleakley C.M., Selfe J. and Donnelly A.E. The use of thermal imaging in assessing skin temperature following cryotherapy: a review. *J. Thermal Biology* (2012) **37**:103–110.

[8] Cramer K.E., Howell P.A. and Syed H.I. Quantitative thermal imaging of aircraft structures. *Proc. SPIE Thermosense XVII* (1995) **2473**: num. 226232.

[9] Eaton J. W., Bateman D., Hauberg S. and Wehbring R. GNU Octave version 4.0.0 manual: a high-level interactive language for numerical computations. (2015). URL http://www.gnu.org/software/octave/doc/interpreter/

[10] Funes J.F., Perales J.M., Rapún M.-L. and J.M. Vega. Defect detection from multifrequency limited data via topological sensitivity. *J. Math. Imaging Vis.* (2016) **55**:19–35.

[11] Guzina B.B. and Bonnet M. Small-inclusion asymptotic of misfit functionals for inverse problems in acoustics. *Inverse Problems* (2006) **22**:1761–1785.

[12] Hecht, F. New development in FreeFem++. *J. Numer. Math.* (2012), **20**: 251–265.

[13] Kylili A., Fokaides P.A., Christou P. and Kalogirou S.A. Infrared thermography (IRT) applications for building diagnosis: a review. *Applied Energy* (2014) **134**:531–549.

[14] Le Loüer F. and Rapún M.-L. Topological sensitivity for solving inverse multiple scattering problems in three-dimensional electromagnetism. Part I: One step method. *SIAM J. Imaging Sciences* (2017) **10**: 1291-1321.

[15] Moghbel M. and Mashohor S. A review of computer assisted detection/diagnosis (CAD) in breast thermography for breast cancer detection. *Artif. Intell. Rev.* (2013) **39**:305-313.

[16] Oscher S. and Fedkiw R. *Level set methods and dynamic implicit surfaces.* Applied Mathematical Sciences, vol. 153. Springer-Verlag, New York, 2003.

[17] Park W.K. Topological derivatives strategy for one-step iteration imaging of arbitrary shaped thin, curve-like electromagnetic inclusions. *J. Comput. Phys.* (2012) **231**:1426–1439.

[18] Sokolowski, J. and Zochowski, A. On the topological derivative in shape optimization. *SIAM journal on control and optimization* (1999) **37(4)**:1251–1272.

[19] Syed H.I., Winfree W., Cramer E. and Howell P.A. Thermographic detection of corrosion in aircraft skin. *Review of progress in quantitative nondestructive evaluation* (1993) 2035–2041.

[20] Thành N.T., Sahli H. and Hào D.N. Detection and characterization of buried landmines using infrared thermography. *Inverse Proble. Sci. Eng.* (2011) **19**: 281-307.

[21] Usamentiaga R., Venegas P., Guerediaga J., Vega L., Molleda J. and Bulnes F.G. Infrared thermography for temperature measurement and non-destructive testing. *Sensors* (2014) **14**:12305–12348.